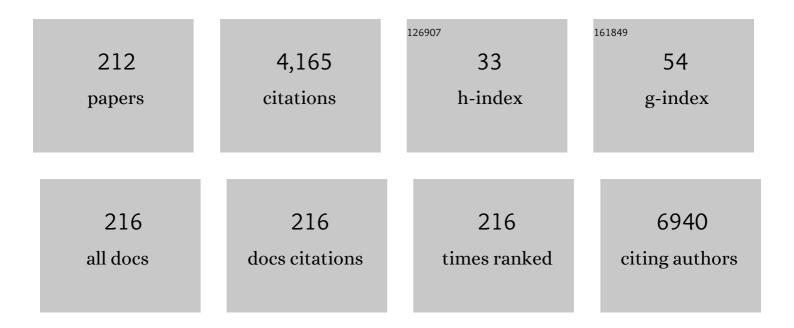
List of Publications by Year in descending order

Source: https://exaly.com/author-pdf/1453205/publications.pdf Version: 2024-02-01



#	Article	IF	CITATIONS
1	Rubicon inhibits autophagy and accelerates hepatocyte apoptosis and lipid accumulation in nonalcoholic fatty liver disease in mice. Hepatology, 2016, 64, 1994-2014.	7.3	264
2	Suppression of allergic inflammation by the prostaglandin E receptor subtype EP3. Nature Immunology, 2005, 6, 524-531.	14.5	215
3	Mast cell maturation is driven via a group III phospholipase A2-prostaglandin D2–DP1 receptor paracrine axis. Nature Immunology, 2013, 14, 554-563.	14.5	122
4	Crucial role for autophagy in degranulation of mast cells. Journal of Allergy and Clinical Immunology, 2011, 127, 1267-1276.e6.	2.9	120
5	Prostaglandin E2–EP3 Signaling Induces Inflammatory Swelling by Mast Cell Activation. Journal of Immunology, 2014, 192, 1130-1137.	0.8	120
6	Modification of BN nanosheets and their thermal conducting properties in nanocomposite film with polysiloxane according to the orientation of BN. Composites Science and Technology, 2011, 71, 1046-1052.	7.8	105
7	Prostaglandin E2 Receptors, EP2 and EP4, Differentially Modulate TNF-α and IL-6 Production Induced by Lipopolysaccharide in Mouse Peritoneal Neutrophils. Biochemical and Biophysical Research Communications, 2000, 278, 224-228.	2.1	89
8	Orientation distribution-Lotgering factor relationship in a polycrystalline material-as an example of bismuth titanate prepared by a magnetic field. Journal of the Ceramic Society of Japan, 2010, 118, 921-926.	1.1	84
9	Gastric acid secretion in L-histidine decarboxylase–deficient mice. Gastroenterology, 2002, 122, 145-155.	1.3	82
10	T helper 2 and regulatory T-cell cytokine production by mast cells: a key factor in the pathogenesis of IgG4-related disease. Modern Pathology, 2014, 27, 1126-1136.	5.5	79
11	Particle Oriented Bismuth Titanate Ceramics Made in High Magnetic Field. Journal of the Ceramic Society of Japan, 2003, 111, 702-704.	1.3	72
12	Antigen-independent Induction of Histamine Synthesis by Immunoglobulin E in Mouse Bone Marrow–derived Mast Cells. Journal of Experimental Medicine, 2002, 196, 229-235.	8.5	70
13	Expression of Messenger RNA for Prostaglandin E Receptor Subtypes EP4/EP2 and Cyclooxygenase Isozymes in Mouse Periovulatory Follicles and Oviducts During Superovulation1. Biology of Reproduction, 2003, 68, 804-811.	2.7	70
14	Fabrication of c-axis oriented polycrystalline ZnO by using a rotating magnetic field and following sintering. Journal of Materials Research, 2006, 21, 703-707.	2.6	62
15	Facile preparation of a polysiloxane-based hybrid composite with highly-oriented boron nitride nanosheets and an unmodified surface. Composites Science and Technology, 2010, 70, 1681-1686.	7.8	59
16	Bak deficiency inhibits liver carcinogenesis: A causal link between apoptosis and carcinogenesis. Journal of Hepatology, 2012, 57, 92-100.	3.7	54
17	Orientation dependence of transport property and microstructural characterization of Al-doped ZnO ceramics. Acta Materialia, 2007, 55, 4753-4757.	7.9	49
18	Self-assemblies of linearly aligned diamond fillers in polysiloxane/diamond composite films with enhanced thermal conductivity. Composites Science and Technology, 2011, 72, 112-118.	7.8	49

#	Article	IF	CITATIONS
19	Ca ²⁺ influxâ€mediated histamine synthesis and ILâ€6 release in mast cells activated by monomeric IgE. European Journal of Immunology, 2005, 35, 460-468.	2.9	47
20	Sintering deformation caused by particle orientation in uniaxially and isostatically pressed alumina compacts. Journal of the European Ceramic Society, 2002, 22, 311-316.	5.7	43
21	Crucial Role of Histamine for Regulation of Gastric Acid Secretion Ascertained by Histidine Decarboxylase-Knockout Mice. Journal of Pharmacology and Experimental Therapeutics, 2003, 307, 331-338.	2.5	42
22	DNase II activated by the mitochondrial apoptotic pathway regulates RIP1-dependent non-apoptotic hepatocyte death via the TLR9/IFN-β signaling pathway. Cell Death and Differentiation, 2019, 26, 470-486.	11.2	42
23	ST6GAL1 Is a Novel Serum Biomarker for Lenvatinib-Susceptible FGF19-Driven Hepatocellular Carcinoma. Clinical Cancer Research, 2021, 27, 1150-1161.	7.0	42
24	Effect of Cimetidine on Intratumoral Cytokine Expression in an Experimental Tumor. Biochemical and Biophysical Research Communications, 2001, 281, 1113-1119.	2.1	41
25	Interface topology for distinguishing stages of sintering. Scientific Reports, 2017, 7, 11106.	3.3	41
26	Recent Advances in Molecular Pharmacology of the Histamine Systems: Immune Regulatory Roles of Histamine Produced by Leukocytes. Journal of Pharmacological Sciences, 2006, 101, 19-23.	2.5	40
27	Expression ofL-histidine decarboxylase in granules of elicited mouse polymorphonuclear leukocytes. European Journal of Immunology, 2004, 34, 1472-1482.	2.9	39
28	C-Axis Orientation of KSr2Nb5O15Using a Rotating Magnetic Field. Journal of the American Ceramic Society, 2007, 90, 3503-3506.	3.8	39
29	Establishment of the culture model system that reflects the process of terminal differentiation of connective tissueâ€ŧype mast cells. FEBS Letters, 2008, 582, 1444-1450.	2.8	38
30	Interleukin-6 Is a Circulating Prognostic Biomarker for Hepatocellular Carcinoma Patients Treated with Combined Immunotherapy. Cancers, 2022, 14, 883.	3.7	38
31	Activation of Histidine Decarboxylase through Post-translational Cleavage by Caspase-9 in a Mouse Mastocytoma P-815. Journal of Biological Chemistry, 2007, 282, 13438-13446.	3.4	37
32	Crystal-Oriented Bi4Ti3O12Ceramics Fabricated by High-Magnetic-Field Method. Japanese Journal of Applied Physics, 2004, 43, 6645-6648.	1.5	36
33	Expression of l-Histidine Decarboxylase in Mouse Male Germ Cells. Journal of Biological Chemistry, 2002, 277, 14211-14215.	3.4	34
34	Fabrication of c-axis Oriented Zn0.98Al0.02O by a High-Magnetic-Field via Gelcasting and its Thermoelectric Properties. Journal of the Ceramic Society of Japan, 2006, 114, 1085-1088.	1.3	34
35	Strengthâ€Processing Defects Relationship Based on Micrographic Analysis and Fracture Mechanics in Alumina Ceramics. Journal of the American Ceramic Society, 2009, 92, 688-693.	3.8	34
36	Emergence of hepatitis C virus NS5A L31V plus Y93H variant upon treatment failure of daclatasvir and asunaprevir is relatively resistant to ledipasvir and NS5B polymerase nucleotide inhibitor GS-558093 in human hepatocyte chimeric mice. Journal of Gastroenterology, 2015, 50, 1145-1151.	5.1	33

#	Article	IF	CITATIONS
37	Effect of Organic Binder Segregation on Sintered Strength of Dry-Pressed Alumina. Journal of the American Ceramic Society, 2006, 89, 1903-1907.	3.8	31
38	Critical role of endogenous histamine in promoting end-organ tissue injury in sepsis. Intensive Care Medicine Experimental, 2016, 4, 36.	1.9	31
39	Coarse pore evolution in dry-pressed alumina ceramics during sintering. Advanced Powder Technology, 2016, 27, 1006-1012.	4.1	31
40	Possible coupling of prostaglandin E receptor EP1 to TRP5 expressed in Xenopus laevis oocytes. Biochemical and Biophysical Research Communications, 2002, 298, 398-402.	2.1	30
41	Preparation and Thermoelectric Property of Highly Oriented Al-Doped ZnO Ceramics by a High Magnetic Field. Japanese Journal of Applied Physics, 2006, 45, L1212-L1214.	1.5	30
42	Linear Assembles of BN Nanosheets, Fabricated in Polymer/BN Nanosheet Composite Film. Journal of Nanomaterials, 2011, 2011, 1-7.	2.7	30
43	Effect of internal binder on microstructure in compacts made from granules. Journal of the European Ceramic Society, 2007, 27, 873-877.	5.7	28
44	Epoxy resin-based nanocomposite films with highly oriented BN nanosheets prepared using a nanosecond-pulse electric field. Materials Letters, 2011, 65, 2426-2428.	2.6	28
45	Facile orientation of unmodified BN nanosheets in polysiloxane/BN composite films using a high magnetic field. Journal of Materials Science, 2011, 46, 2318-2323.	3.7	27
46	S100A8 Production in CXCR2-Expressing CD11b+Gr-1high Cells Aggravates Hepatitis in Mice Fed a High-Fat and High-Cholesterol Diet. Journal of Immunology, 2016, 196, 395-406.	0.8	27
47	3D multiscale-imaging of processing-induced defects formed during sintering of hierarchical powder packings. Scientific Reports, 2019, 9, 11595.	3.3	27
48	Carbamazepine promotes liver regeneration and survival in mice. Journal of Hepatology, 2013, 59, 1239-1245.	3.7	26
49	Fabrication of transparent crystal-oriented polycrystalline strontium barium niobate ceramics for electro-optical application. Journal of the European Ceramic Society, 2014, 34, 3723-3728.	5.7	26
50	Vesicular Polyamine Transporter Mediates Vesicular Storage and Release of Polyamine from Mast Cells. Journal of Biological Chemistry, 2017, 292, 3909-3918.	3.4	26
51	Roles of IgE and Histamine in Mast Cell Maturation. Cells, 2021, 10, 2170.	4.1	26
52	c-axis oriented ZnO formed in a rotating magnetic field with various rotation speeds. Journal of the European Ceramic Society, 2009, 29, 955-959.	5.7	25
53	Lack of histamine alters gastric mucosal morphology: comparison of histidine decarboxylase-deficient and mast cell-deficient mice. American Journal of Physiology - Renal Physiology, 2004, 287, G1053-G1061.	3.4	24
54	Intensity-modulated radiation therapy with concurrent chemotherapy followed by durvalumab for stage III non-small cell lung cancer: A multi-center retrospective study. Radiotherapy and Oncology, 2021, 160, 266-272.	0.6	24

#	Article	IF	CITATIONS
55	Crystal-Oriented La-Substituted Sr2NaNb5O15Ceramics Fabricated Using High-Magnetic-Field Method. Japanese Journal of Applied Physics, 2006, 45, 7460-7464.	1.5	23
56	Cell Surface-Anchored Fluorescent Probe Capable of Real-Time Imaging of Single Mast Cell Degranulation Based on Histamine-Induced Coordination Displacement. Analytical Chemistry, 2016, 88, 1526-1529.	6.5	23
57	Extracellular ATP Augments Antigen-Induced Murine Mast Cell Degranulation and Allergic Responses via P2X4 Receptor Activation. Journal of Immunology, 2020, 204, 3077-3085.	0.8	23
58	C-axis-Oriented (Sr,Ca) ₂ NaNb ₅ O ₁₅ Multilayer Piezoelectric Ceramics Fabricated Using High-Magnetic-Field Method. Japanese Journal of Applied Physics, 2008, 47, 7693.	1.5	22
59	Identification and characterization of a novel progesterone receptor-binding element in the mouse prostaglandin E receptor subtype EP2 gene. Genes To Cells, 2003, 8, 747-758.	1.2	21
60	Noise-robust transparent visualization of large-scale point clouds acquired by laser scanning. ISPRS Journal of Photogrammetry and Remote Sensing, 2020, 161, 124-134.	11.1	21
61	Clinical factors associated with shorter durable response, and patterns of acquired resistance to first-line pembrolizumab monotherapy in PD-L1-positive non-small-cell lung cancer patients: a retrospective multicenter study. BMC Cancer, 2021, 21, 346.	2.6	21
62	Kinetics of property change associated with atmospheric humidity changes in alumina powder granules with PVA binder. Journal of the European Ceramic Society, 2002, 22, 2835-2840.	5.7	20
63	Induction of Adherent Activity in Mastocytoma P-815 Cells by the Cooperation of Two Prostaglandin E2 Receptor Subtypes, EP3 and EP4. Journal of Biological Chemistry, 2003, 278, 17977-17981.	3.4	20
64	Uptake of histamine by mouse peritoneal macrophages and a macrophage cell line, RAW264.7. American Journal of Physiology - Cell Physiology, 2003, 285, C592-C598.	4.6	20
65	Particle Oriented Strontium Bismuth Titanate Ceramics Prepared by Using High Magnetic Field and Subsequent Reaction Sintering. Journal of the Ceramic Society of Japan, 2007, 115, 237-240.	1.3	20
66	Computation of sintering stress and bulk viscosity from microtomographic images in viscous sintering of glass particles. Journal of the American Ceramic Society, 2017, 100, 867-875.	3.8	20
67	Fabrication of <i>c</i> -axis oriented higher manganese silicide by a high-magnetic-field and its thermoelectric properties. Journal of Materials Research, 2007, 22, 2917-2923.	2.6	19
68	Involvement of CD44 in mast cell proliferation during terminal differentiation. Laboratory Investigation, 2009, 89, 446-455.	3.7	19
69	Microstructural Evidence of Hall Mobility Anisotropy in c-Axis Textured Al-Doped ZnO. Journal of the American Ceramic Society, 2011, 94, 2339-2343.	3.8	19
70	Sodium taurocholate cotransporting polypeptide inhibition efficiently blocks hepatitis B virus spread in mice with a humanized liver. Scientific Reports, 2016, 6, 27782.	3.3	19
71	Infrared Microscopy for Examination of Structure in Sprayâ€Dried Granules and Compacts. Journal of the American Ceramic Society, 2001, 84, 254-256.	3.8	18
72	Particle Orientation Distribution in Alumina Compact Body Prepared by the Slip Casting Method. Journal of the Ceramic Society of Japan, 2004, 112, 276-279.	1.3	18

#	Article	IF	CITATIONS
73	Prostaglandin EP3 receptor superactivates adenylyl cyclase via the Gq/PLC/Ca2+ pathway in a lipid raft-dependent manner. Biochemical and Biophysical Research Communications, 2009, 389, 678-682.	2.1	18
74	Fabrication of c-axis-oriented potassium strontium niobate (KSr2Nb5O15) ceramics by a rotating magnetic field and electrical property. Journal of the Ceramic Society of Japan, 2010, 118, 722-725.	1.1	18
75	Fabrication of Transparent Grainâ€Oriented Polycrystalline Alumina by Colloidal Processing. Journal of the American Ceramic Society, 2016, 99, 3217-3219.	3.8	18
76	Critical Role of Protein Kinase C βII in Activation of Mast Cells by Monomeric IgE. Journal of Biological Chemistry, 2005, 280, 38976-38981.	3.4	17
77	A quantitative evaluation method for particle orientation structure in alumina powder compacts. Journal of the European Ceramic Society, 2007, 27, 3399-3406.	5.7	17
78	Neuromedin U directly induces degranulation of skin mast cells, presumably via <scp>MRGPRX</scp> 2. Allergy: European Journal of Allergy and Clinical Immunology, 2018, 73, 2256-2260.	5.7	17
79	Direct observation of aggregates and agglomerates in alumina granules. Powder Technology, 2003, 129, 153-155.	4.2	16
80	Fabrication of crystal-oriented barium-bismuth titanate ceramics in high magnetic field and subsequent reaction sintering. Science and Technology of Advanced Materials, 2009, 10, 014602.	6.1	16
81	Effect of Cold Isostatic Pressing on Microstructure and Shrinkage Anisotropy during Sintering of Uniaxially Pressed Alumina Compacts Journal of the Ceramic Society of Japan, 2002, 110, 264-269.	1.3	15
82	Thermal anisotropy of epoxy resin-based nano-hybrid films containing BN nanosheets under a rotating superconducting magnetic field. Materials Chemistry and Physics, 2013, 139, 355-359.	4.0	15
83	Influence of binder layer of spray-dried granules on occurrence and evolution of coarse defects in alumina ceramics during sintering. Journal of the European Ceramic Society, 2018, 38, 1846-1852.	5.7	15
84	Direct Evidence for Lowâ€Density Regions in Compacted Sprayâ€Dried Powders. Journal of the American Ceramic Society, 2001, 84, 2454-2456.	3.8	14
85	Essential role of EP3 subtype in prostaglandin E ₂ -induced adhesion of mouse cultured and peritoneal mast cells to the Arg-Cly-Asp-enriched matrix. American Journal of Physiology - Cell Physiology, 2008, 295, C1427-C1433.	4.6	14
86	Estimation of Weibull modulus from coarser defect distribution in dry-pressed alumina ceramics. Journal of the Ceramic Society of Japan, 2009, 117, 742-747.	1.1	14
87	PARTICLE-BASED TRANSPARENT FUSED VISUALIZATION APPLIED TO MEDICAL VOLUME DATA. International Journal of Modeling, Simulation, and Scientific Computing, 2013, 04, 1341003.	1.4	14
88	The Bcl-2 Homology Domain 3 (BH3)-only Proteins Bim and Bid Are Functionally Active and Restrained by Anti-apoptotic Bcl-2 Family Proteins in Healthy Liver*. Journal of Biological Chemistry, 2013, 288, 30009-30018.	3.4	14
89	Particle sedimentation monitoring in high-concentration slurries. AIP Advances, 2016, 6, .	1.3	14
90	A Cluster of Aromatic Amino Acids in the i2 Loop Plays a Key Role for Gs Coupling in Prostaglandin EP2 and EP3 Recentors, Journal of Biological Chemistry, 2004, 279, 11016-11026	3.4	13

#	Article	IF	CITATIONS
91	Chemical Genetic Identification of the Histamine H1 Receptor as a Stimulator of Insulin-Induced Adipogenesis. Chemistry and Biology, 2004, 11, 907-913.	6.0	13
92	Development of eosinophilic conjunctival inflammation at late-phase reaction in mast cell–deficient mice. Journal of Allergy and Clinical Immunology, 2007, 120, 476-478.	2.9	13
93	Characterization of gene expression profiles for different types of mast cells pooled from mouse stomach subregions by an RNA amplification method. BMC Genomics, 2009, 10, 35.	2.8	13
94	Electric-field-assisted fabrication of linearly stretched bundles of microdiamonds in polysiloxane-based composite material. Diamond and Related Materials, 2012, 26, 7-14.	3.9	13
95	Retinal Vessel Segmentation via a Semantics and Multi-Scale Aggregation Network. , 2020, , .		13
96	Functional domains essential for Gs activity in prostaglandin EP2 and EP3 receptors. Life Sciences, 2003, 74, 135-141.	4.3	12
97	Packing Structure of Particles in a Green Compact and Its Influence on Sintering Deformation. Journal of the American Ceramic Society, 2007, 90, 3717-3719.	3.8	12
98	Synthetic lethal interaction of combined <scp>CD26</scp> and <scp>Bclâ€xL</scp> inhibition is a powerful anticancer therapy against hepatocellular carcinoma. Hepatology Research, 2015, 45, 1023-1033.	3.4	12
99	Colloidal processing using UV curable resin under high magnetic field for textured ceramics. Journal of the European Ceramic Society, 2016, 36, 2739-2743.	5.7	12
100	Two-Step Differentiation of Mast Cells from Induced Pluripotent Stem Cells. Stem Cells and Development, 2013, 22, 726-734.	2.1	11
101	The effect of packing structure of powder particles on warping during sintering. Journal of the European Ceramic Society, 2008, 28, 21-25.	5.7	10
102	Hepatitis B virus reactivation associated with temozolomide for malignant glioma: a case report and recommendation for prophylaxis. International Journal of Clinical Oncology, 2012, 17, 290-293.	2.2	10
103	3D reconstruction of Borobudur reliefs from 2D monocular photographs based on soft-edge enhanced deep learning. ISPRS Journal of Photogrammetry and Remote Sensing, 2022, 183, 439-450.	11.1	10
104	Preparation and saponification of vinyl siloxane—Vinyl acetate copolymers. Polymer, 1986, 27, 123-128.	3.8	9
105	Evolution of Discontinuity in Particle Orientation in Ceramic Tape Casting. Journal of the American Ceramic Society, 2008, 91, 3181-3184.	3.8	9
106	High-Power Piezoelectric Characteristics of C-Axis Crystal-Oriented (Sr,Ca) ₂ NaNb ₅ O ₁₅ Ceramics. Japanese Journal of Applied Physics, 2012, 51, 09LD02.	1.5	9
107	Evaluation of dispersability of gamma alumina prepared by homogeneous precipitation. Journal of the Ceramic Society of Japan, 2012, 120, 290-294.	1.1	9
108	Densely Packed Linear Assembles of Carbon Nanotube Bundles in Polysiloxane-Based Nanocomposite Films. Journal of Nanomaterials, 2013, 2013, 1-10.	2.7	9

#	Article	IF	CITATIONS
	Crystal-oriented (Bi _{0.5} ,) Tj ETQq1 1 0.784314 rgBT /Overlock 10 Tf 50 752 Td (Na<	sub>0.5&l	t;/sub>)&
109	ceramics prepared by colloidal processing in rotating high magnetic field. Journal of the Ceramic Society of Japan, 2015, 123, 340-344.	1.1	9
110	High-power properties of crystal-oriented (Sr,Ca) ₂ NaNb ₅ O ₁₅ piezoelectric ceramics and their application to ultrasonic motors. Japanese Journal of Applied Physics, 2019, 58, SGGA07.	1.5	9
111	Suppression of IgE-Independent Degranulation of Murine Connective Tissue-Type Mast Cells by Dexamethasone. Cells, 2019, 8, 112.	4.1	9
112	Fabrication of c-axis oriented hydroxyapatite ceramics in a rotating high magnetic field using photopolymerization. Journal of the European Ceramic Society, 2020, 40, 4332-4339.	5.7	9
113	Effect of Segregation of a Polyacrylic Acid (PAA) Binder on the Green Strength of Dryâ€Pressed Alumina Compacts. Journal of the American Ceramic Society, 2008, 91, 3896-3902.	3.8	8
114	Effect of polyacrylic acid (PAA) binder system on particle orientation during dry-pressing. Powder Technology, 2009, 196, 133-138.	4.2	8
115	Targeting CD44 in mast cell regulation. Expert Opinion on Therapeutic Targets, 2010, 14, 31-43.	3.4	8
116	Formation and Structural Characteristic of Perpendicularly Aligned Boron Nitride Nanosheet Bridges in Polymer/Boron Nitride Composite Film and Its Thermal Conductivity. Japanese Journal of Applied Physics, 2011, 50, 01BJ05.	1.5	8
117	Fabrication of c-axis oriented Si3N4 ceramics using multilayered-graphene-coated β-Si3N4 seeds and their orientation in an innovative low magnetic field. Advanced Powder Technology, 2016, 27, 2005-2011.	4.1	8
118	Fused Transparent Visualization of Point Cloud Data and Background Photographic Image for Tangible Cultural Heritage Assets. ISPRS International Journal of Geo-Information, 2019, 8, 343.	2.9	8
119	Prolonged Gut Dysbiosis and Fecal Excretion of Hepatitis A Virus in Patients Infected with Human Immunodeficiency Virus. Viruses, 2021, 13, 2101.	3.3	8
120	Volume Rendering Using Tiny Particles. , 2006, , .		7
121	Development of Packing Structure of Powder Particles in Tape Casting. Journal of the Ceramic Society of Japan, 2007, 115, 136-140.	1.3	7
122	Stochastic analysis on ceramic granule collapse in powder compact during cold isostatic pressing. Advanced Powder Technology, 2016, 27, 940-947.	4.1	7
123	1â€Fluoroâ€2,4â€dinitrobenzene and its derivatives act as secretagogues on rodent mast cells. European Journal of Immunology, 2017, 47, 60-67.	2.9	7
124	A case of simultaneous occurrence of hepatitis and pancreatitis during the combination immunochemotherapy for non-small cell lung carcinoma. Respiratory Medicine Case Reports, 2020, 31, 101266.	0.4	7
125	Establishment and Characterization of a Murine Mucosal Mast Cell Culture Model. International Journal of Molecular Sciences, 2020, 21, 236.	4.1	7
126	Morphological Change of Large Pores in Alumina Ceramics in the Final Stage of Densification. Journal of the Ceramic Society of Japan, 2003, 111, 525-527.	1.3	6

SATOSHI ΤΑΝΑΚΑ

#	Article	IF	CITATIONS
127	Design of Packing Structures through Direct Characterization of Ceramics Green Bodies. Journal of the Ceramic Society of Japan, 2006, 114, 141-146.	1.3	6
128	Molecular orbital approach to the optical nonlinearities of fresnoite-type crystals. Journal of the European Ceramic Society, 2007, 27, 531-533.	5.7	6
129	Fabrication of highly particle-oriented alumina green compact from non-aqueous slurry. Journal of the Ceramic Society of Japan, 2011, 119, 198-202.	1.1	6
130	Enhancing the contrast of low-density packing regions in images of ceramic powder compacts using a contrast agent for micro-X-ray computed tomography. Journal of the Ceramic Society of Japan, 2014, 122, 574-576.	1.1	6
131	Photorealistic VR Space Reproductions of Historical Kyoto Sites based on a Next-Generation 3D Game Engine. Journal of Advanced Simulation in Science and Engineering, 2015, 1, 188-204.	0.2	6
132	Surface crystallization and gas bubble formation during conventional heat treatment in Na2MnP2O7 glass. Journal of Non-Crystalline Solids, 2019, 510, 36-41.	3.1	6
133	Possible Contribution of Inflammation-Associated Hypoxia to Increased K2P5.1 K+ Channel Expression in CD4+ T Cells of the Mouse Model for Inflammatory Bowel Disease. International Journal of Molecular Sciences, 2020, 21, 38.	4.1	6
134	High-power properties of (Sr,Ca)2NaNb5O15piezoelectric ceramics in a longitudinal mode. Japanese Journal of Applied Physics, 2020, 59, SKKA07.	1.5	6
135	Phenotypic and Functional Diversity of Mast Cells. International Journal of Molecular Sciences, 2020, 21, 3835.	4.1	6
136	Toughening of carbon fiber/pitch-based carbon matrix composites by microspace control. Synthetic Metals, 2001, 125, 213-221.	3.9	5
137	Infrared Microscopy as a Powerful Tool for the Examination of Internal Microstructure of Nano-Powder Compact-Yittria Stabilized Zirconia as a Model Journal of the Ceramic Society of Japan, 2004, 112, 114-116.	1.3	5
138	Polyepoxide-based nanohybrid films with self-assembled linear assemblies of nanodiamonds. Acta Materialia, 2012, 60, 7249-7257.	7.9	5
139	Mitogen-activated protein kinases-dependent induction of hepatocyte growth factor production in human dermal fibroblasts by the antibiotic polymyxin B. Cytokine, 2012, 60, 205-211.	3.2	5
140	Real-time isosurface rendering of smooth fields. Journal of Visualization, 2012, 15, 179-187.	1.8	5
141	Anisotropic sintering behavior of grain-oriented strontium barium niobate ceramics. Journal of the Ceramic Society of Japan, 2013, 121, 411-415.	1.1	5
142	Observation of Particle Motion in High oncentration Ceramic Slurries Under Low Shear Rate. Journal of the American Ceramic Society, 2015, 98, 1429-1436.	3.8	5
143	Particle Rotation in Colloidal Processing under a Strong Rotating Magnetic Field. Langmuir, 2018, 34, 6462-6469.	3.5	5
144	Influence of tetragonality on crystal orientation induced by a strong magnetic field and on the piezoelectric properties of the (Bi _{0.5} ,) Tj ETQq0 0 0 rgBT /Overlock 10 Tf 50 62 Td (Na _{0.5<td>ıb_{})}sub></td><td> 1ą̂_`'</td>} <i< td=""></i<>	ıb _{})} sub>	 1ą̂_`'

system. Journal of the Ceramic Society of Japan, 2018, 126, 655-661.

#	Article	IF	CITATIONS
145	Ligation of MHC Class II Induces PKC-Dependent Clathrin-Mediated Endocytosis of MHC Class II. Cells, 2020, 9, 1810.	4.1	5
146	Drug-Induced Kidney Injury Caused by Osimertinib: Report of a Rare Case. Nephron, 2022, 146, 58-63.	1.8	5
147	Domain coarsening in viscous sintering as a result of topological pore evolution. Journal of the European Ceramic Society, 2022, 42, 729-733.	5.7	5
148	Influence of Dehydration Rate on the Degree of Particle Orientation in Alumina Green Body Made by Slip Casting. Journal of the Ceramic Society of Japan, 2004, 112, 641-645.	1.3	4
149	Observation of the granule packing structure using a confocal laser-scanning microscope. Journal of the European Ceramic Society, 2006, 26, 683-687.	5.7	4
150	Compatibility of PVB of Mixed Organic Solvents in Alumina Slurries and its Effect on Morphology of Green Sheets. Journal of the American Ceramic Society, 2011, 94, 2819-2824.	3.8	4
151	Quantitative analysis of de-aggregation behavior in alumina suspension by beads milling. Powder Technology, 2012, 217, 619-623.	4.2	4
152	Dextran sulfate-induced degradation of spontaneously apoptotic B cells. International Immunopharmacology, 2013, 15, 581-587.	3.8	4
153	Highlighting Feature Regions Combined with See-Through Visualization of Laser-Scanned Cultural Heritage. , 2017, , .		4
154	Effects of ammonium molybdate additive and sintering temperature on the properties of foam ceramics based on ceramic tile polishing waste. Journal of the Ceramic Society of Japan, 2019, 127, 318-326.	1.1	4
155	Anisotropic sintering shrinkage and microstructural evolution of <i>c</i> -axis-oriented Si ₃ N ₄ ceramics. Journal of the Ceramic Society of Japan, 2019, 127, 435-442.	1.1	4
156	gMocren: High-quality volume visualization tool for Geant4 simulation. , 2007, , .		3
157	Piezoelectric Properties of <i>c</i> -Axis-Oriented (Sr,Ca) ₂ NaNb ₅ O ₁₅ Piezoelectric Ceramics with Single-Plate Type and Multilayered Type Fabricated Using Crystal-Oriented Sheet Forming, Key Engineering Materials, 0, 421-422, 21-25.	0.4	3
158	Data fitting independent of grid structure using a volumic version of MPU. Journal of Visualization, 2011, 14, 161-170.	1.8	3
159	Influence of Aggregates in αâ€ <scp><scp>Al</scp></scp> ₂ <scp><scp>O</scp></scp> ₃ Slurry on Orientation Degree of Powder Compact Fabricated by Magnetic Forming Method. Journal of the American Ceramic Society. 2013. 96. 2411-2418.	3.8	3
160	Visual Point-Based Analysis of Laser-Scanned Historical Structures. , 2015, , .		3
161	Influence of granule characteristics on fabrication of translucent alumina ceramics with high strength and reliability. Journal of the Ceramic Society of Japan, 2016, 124, 426-431.	1.1	3
162	Down-modulation of antigen-induced activation of murine cultured mast cells sensitized with a highly cytokinergic IgE clone. Immunology Letters, 2016, 174, 1-8.	2.5	3

#	Article	IF	CITATIONS
163	Improving Transparent Visualization of Large-Scale Laser-Scanned Point Clouds by Using Poisson Disk Sampling. , 2017, , .		3
164	Suppression of IFN-Î ³ Production in Murine Splenocytes by Histamine Receptor Antagonists. International Journal of Molecular Sciences, 2018, 19, 4083.	4.1	3
165	Deep Learning-Based Point Upsampling for Edge Enhancement of 3D-Scanned Data and Its Application to Transparent Visualization. Remote Sensing, 2021, 13, 2526.	4.0	3
166	Visualization of riverine water and vortex dynamics around the Naruto Strait based on high-resolution ocean simulation and satellite images. Journal of Advanced Simulation in Science and Engineering, 2020, 7, 214-225.	0.2	3
167	Characterization of Internal Structure of a Green Body Made by Dry-Pressing. Key Engineering Materials, 2004, 264-268, 189-192.	0.4	2
168	Evaluation of Bubble Content in Aqueous Alumina Slurries. Journal of the Ceramic Society of Japan, 2005, 113, 449-451.	1.3	2
169	Requirements in modeling and visualization for Geant4-based radiotherapy simulation. , 2007, , .		2
170	Preprocessing for Accelerating Convergence of Repulsive-Particle Systems for Sampling Implicit Surfaces. , 2007, , .		2
171	Automatic Modeling of Virtual 3D Streets Based on GIS Data - Application to Generation of Kyoto in the Edo Era. , 2009, , .		2
172	Suppression of CXCR4 expression in mast cells upon IgE-mediated antigen stimulation. Inflammation Research, 2010, 59, 123-127.	4.0	2
173	MESHFREE ELASTODYNAMIC ANALYSIS OF THREE-DIMENSIONAL SOLIDS USING RADIAL POINT INTERPOLATION METHOD. International Journal of Modeling, Simulation, and Scientific Computing, 2011, 02, 83-95.	1.4	2
174	Determination of sintering stress and bulk viscosity from sinter-forging and X-ray microtomography methods: a Review. Materials Today: Proceedings, 2019, 16, 42-48.	1.8	2
175	Preparation and gas permeance of c-axis oriented zeolite membrane using ion-exchanged mordenite zeolite crystals oriented in magnetic field. Journal of the European Ceramic Society, 2020, 40, 5984-5990.	5.7	2
176	Translucent Visual Analysis of Large Scale 3D Point Data Generated by Particle Fluid Simulation of Tsunami Water. Journal of Advanced Simulation in Science and Engineering, 2014, 1, 5-15.	0.2	2
177	Direct observation of the deformation behavior of agglomerates in a highly concentrated slurry under startup shear flow. Open Ceramics, 2022, 9, 100209.	2.0	2
178	Fractography for Alumina Ceramics Using a Confocal Scanning Laser Microscope Journal of the Ceramic Society of Japan, 2001, 109, 1055-1056.	1.3	1
179	Influence of microstructure on modal work-of-fracture of carbon fibre/pitch-derived carbon composites. International Journal of Materials and Product Technology, 2001, 16, 171.	0.2	1
180	New characterization method for pore and packing structure in powder compacts using confocal laser scanning microscope. Journal of Electron Microscopy, 2002, 51, 215-223.	0.9	1

#	Article	IF	CITATIONS
181	Meshless structural analyses of complex shape models using implicit surface representations. Journal of Plasma Physics, 2006, 72, 1081.	2.1	1
182	Characteristics of Machining Damage and Their Influence on Strength in Alumina Ceramics System. Key Engineering Materials, 2006, 317-318, 285-288.	0.4	1
183	Zinc Oxide Ceramics with High Mobility as n-Type Thermoelectric Materials. Materials Science Forum, 2007, 561-565, 581-586.	0.3	1
184	A Model for Estimating Internal Stress during Sintering of Ceramic Multiphase Laminates. Key Engineering Materials, 0, 616, 14-18.	0.4	1
185	gMocren: Visualization software for Monte Carlo simulators for radiotherapy. Journal of Advanced Simulation in Science and Engineering, 2015, 2, 45-62.	0.2	1
186	Complicated Flow Behavior of Silica Particles in Concentrated Slurry. Journal of the Society of Powder Technology, Japan, 2016, 53, 294-300.	0.1	1
187	Re-challenge chemotherapy in patients with sensitive relapse small-cell lung cancer and interstitial lung disease. Journal of Thoracic Disease, 2019, 11, 514-520.	1.4	1
188	Transparent Collision Visualization of Point Clouds Acquired by Laser Scanning. ISPRS International Journal of Geo-Information, 2019, 8, 425.	2.9	1
189	Effective oriented direction for enhancement of the piezoelectric properties of crystal-oriented (Li,) Tj ETQq1 1	0.784314 2.3	rgBŢ /Overlo <mark>c</mark> i
190	Development of Functional Ceramics by Colloidal Processing in Rotating High Magnetic Field. Funtai Oyobi Fummatsu Yakin/Journal of the Japan Society of Powder and Powder Metallurgy, 2021, 68, 113-120.	0.2	1
191	Fabrication of Crystal-Oriented Bulk Piezoelectric Ceramics by Stereolithography in Magnetic Field. Funtai Oyobi Fummatsu Yakin/Journal of the Japan Society of Powder and Powder Metallurgy, 2020, 67, 621-628.	0.2	1
192	Integrated High-Definition Visualization of Digital Archives for Borobudur Temple. Remote Sensing, 2021, 13, 5024.	4.0	1
193	Characterization of Surface Condition of Non-Oxide Ceramic Powder by Heat of Immersion. Key Engineering Materials, 2004, 264-268, 77-80.	0.4	0
194	Orientation Factor of Grain Oriented Bismuth Titanate Prepared in High Magnetic Field. Advanced Materials Research, 2006, 11-12, 689-692.	0.3	0
195	Impaired activation of mast cells upon IgE-mediated antigen stimulation in a stroke-prone spontaneously hypertensive rat strain, SHRSP.Z. Immunology Letters, 2010, 128, 74-79.	2.5	Ο
196	Anisotropic sintering of oriented ceramics prepared in a rotating magnetic field. IOP Conference Series: Materials Science and Engineering, 2011, 21, 012008.	0.6	0
197	Structural and Electrical Properties of Lanthanide Substituted-Bismuth Titanate Prepared by Low-Temperature Combustion Synthesis. Advanced Materials Research, 2012, 545, 279-284.	0.3	Ο
198	Controlled Linear Assemblies of Graphite Flakes Anchoring Polysiloxane-Based Nanocomposite Films and Enhancement of Thermal Properties. Japanese Journal of Applied Physics, 2013, 52, 028005.	1.5	0

#	Article	IF	CITATIONS
199	Linear Assembly of Oxidized Surface Treated Nanodiamonds in Polymer-Based Nanohybrids by Electric Field Inducement. Materials Science Forum, 0, 761, 107-111.	0.3	0
200	Stress Estimation for Multiphase Ceramics Laminates During Sintering. Ceramic Engineering and Science Proceedings, 2015, , 101-106.	0.1	0
201	The stochastic highlighting of polygon edges in the transparent visualization of large-scale polygon meshes: application to visualizing a high-energy elementary particle detector. Journal of Statistical Computation and Simulation, 2017, 87, 2560-2571.	1.2	0
202	Evaluation of Macroscopic Mechanical Properties from 3-D Visualization of Microstructure in Sintering. Funtai Oyobi Fummatsu Yakin/Journal of the Japan Society of Powder and Powder Metallurgy, 2017, 64, 495-500.	0.2	0
203	Depth Recognition in 3D Translucent Stereoscopic Imaging of Medical Volumes by Means of a Glasses-Free 3D Display. , 2017, , .		0
204	Graded evolution of anisotropic microstructure during sintering from crystalâ€oriented powder compact. International Journal of Applied Ceramic Technology, 2020, 17, 677-684.	2.1	0
205	Hepatocellular carcinoma in an adult patient with congenital absence of the portal vein type II: A case report. JCH Open, 2020, 4, 766-768.	1.6	0
206	Application of Multiple Iso-Surface Rendering to Improvement of Perceived Depth in Transparent Stereoscopic Visualization. Journal of Advanced Simulation in Science and Engineering, 2021, 8, 128-142.	0.2	0
207	A Case of Nasopharyngeal Mycobacteriosis with Bony Erosion of the External Skull Base. Case Reports in Otolaryngology, 2021, 2021, 1-4.	0.2	0
208	Anisotropic Varistor via Magnetic Texturing. Ceramic Engineering and Science Proceedings, 0, , 163-168.	0.1	0
209	Evaluation of Macroscopic Mechanical Properties from 3-D Visualization of Microstructure in Sintering. Funtai Oyobi Fummatsu Yakin/Journal of the Japan Society of Powder and Powder Metallurgy, 2019, 66, 604-610.	0.2	0
210	Invisiblization of Measurement Noise for Visualization of 3D Scanned Data. Journal of the Visualization Society of Japan, 2021, 41, 7-11.	0.0	0
211	A pneumatocele observed in the thoracic cavity after bronchoalveolar lavage. Journal of Clinical Images and Medical Case Reports, 2021, 2, .	0.0	0
212	Visualization of 3D Scanned Data to Support Sandplay Therapy. Journal of the Visualization Society of Japan, 2021, 41, 2-6.	0.0	0